Chin. Geogra. Sci. 2020 Vol. 30 No. 2 pp. 294–308
https://doi.org/10.1007/s11769-020-1112-5

Springer Science Press
www.springerlink.com/content/1002-0063

Impact of Urban 3D Morphology on Particulate Matter 2.5 ($PM_{2.5}$) Concentrations: Case Study of Beijing, China

LUAN Qingzu[1, 2], JIANG Wei[3, 4], LIU Shuo[5], GUO Hongxiang[5, 6]

(1. *Institute of Urban Meteorology*, *China Meteorological Administration*, *Beijing* 100089, *China*; 2. *Beijing Municipal Climate Center*, *Beijing* 100089, *China*; 3. *China Institute of Water Resources and Hydropower Research*, *Beijing* 100038, *China*; 4. *Research Center of Flood and Drought Disaster Reduction of the Ministry of Water Resources*, *Beijing* 100038, *China*; 5. *Aerospace Information Research Institute*, *Chinese Academy of Sciences*, *Beijing* 100094, *China*; 6. *University of Chinese Academy of Sciences*, *Beijing* 100049, *China*)

Abstract: Urban particulate matter 2.5 ($PM_{2.5}$) pollution and public health are closely related, and concerns regarding $PM_{2.5}$ are widespread. Of the underlying factors, the urban morphology is the most manageable. Therefore, investigations of the impact of urban three-dimensional (3D) morphology on $PM_{2.5}$ concentration have important scientific significance. In this paper, 39 $PM_{2.5}$ monitoring sites of Beijing in China were selected with $PM_{2.5}$ automatic monitoring data that were collected in 2013. This data set was used to analyze the impacts of the meteorological condition and public transportation on $PM_{2.5}$ concentrations. Based on the elimination of the meteorological conditions and public transportation factors, the relationships between urban 3D morphology and $PM_{2.5}$ concentrations are highlighted. Ten urban 3D morphology indices were established to explore the spatial-temporal correlations between the indices and $PM_{2.5}$ concentrations and analyze the impact of urban 3D morphology on the $PM_{2.5}$ concentrations. Results demonstrated that road length density (RLD), road area density (RAD), construction area density (CAD), construction height density (CHD), construction volume density (CVD), construction otherness (CO), and vegetation area density (VAD) have positive impacts on the $PM_{2.5}$ concentrations, whereas water area density (WAD), water fragmentation (WF), and vegetation fragmentation (VF) (except for the 500 m buffer) have negative impacts on the $PM_{2.5}$ concentrations. Moreover, the correlations between the morphology indices and $PM_{2.5}$ concentrations varied with the buffer scale. The findings could lay a foundation for the high-precision spatial-temporal modelling of $PM_{2.5}$ concentrations and the scientific planning of urban 3D spaces by authorities responsible for controlling $PM_{2.5}$ concentrations.

Keywords: urban three-dimensional (3D) morphology; particulate matter 2.5 ($PM_{2.5}$); air pollution; urban planning; Beijing, China

Citation: LUAN Qingzu, JIANG Wei, LIU Shuo, GUO Hongxiang, 2020. Impact of Urban 3D Morphology on Particulate Matter 2.5 ($PM_{2.5}$) Concentrations: Case Study of Beijing, China. *Chinese Geographical Science*, 30(2): 294–308. https://doi.org/10.1007/s11769-020-1112-5

1 Introduction

Air pollution has become a social topic of global concern, especially in developing countries (Westervelt et al., 2016). Over the past four decades, remarkable economic development has been achieved in China. However, urban air pollution is currently becoming more severe. The issue has been a growing concern for the public and the government in China (Wang, 2013; Cao et al., 2016; Chen et al., 2017). Among the several types of pollution, particulate matter 2.5 ($PM_{2.5}$) pollution is attracting the most attention. $PM_{2.5}$ refers to particles

Received date: 2019-01-14; accepted date: 2019-05-10

Foundation item: Under the auspices of National Key Research and Development Program of China (No. 2016YFB0502504), Beijing Excellent Youth Talent Program (No. 2015400018760G294), National Natural Science Foundation of China (No. 41201443, 41001267)

Corresponding author: JIANG Wei. E-mail: jiangwei@radi.ac.cn

with aerodynamic diameters less than 2.5 μm, which are also known as fine particles (Westervelt et al., 2016; Yan and Wu, 2016). Epidemiological studies have shown that $PM_{2.5}$ is significantly related to adverse health effects (Chow et al., 2006; Miller et al., 2007; Seltenrich, 2016), such as cardiopulmonary mortality or morbidity (Lin et al., 2015; Bonyadi et al., 2016). In addition, $PM_{2.5}$ significantly affects atmospheric visibility and the urban landscape (Moore et al., 2007; Vidot et al., 2007; Xian, 2007; Ji et al., 2014; Tao et al., 2014; Meng et al., 2015). Researchers define two types of data for $PM_{2.5}$ (Moore et al., 2007; Vidot et al., 2007). The first type is based on real-time monitoring site data, which have the advantages of long-term observations, accuracy, and diversity (Zhang and Cao, 2015; Ma et al., 2017). Remote sensing data are the second type (Wang et al., 2010; Wu et al., 2016; You et al., 2016). Remote sensing data can cover larger scales than in situ monitoring. Chuersuwan et al. (2000) and Yang et al. (2005) are representative of site monitoring studies. In the study by Chuersuwan et al. (2000), they suggested the importance of transport and atmospheric chemistry (i.e., secondary formation) in $PM_{2.5}$ episodes by collecting time-resolved data across New Jersey from July 1997 to June 1998. The mass concentrations of Al, Si, Ca, Mg, and Fe exhibited similar weekly variations in both Beijing and Shanghai of China (Yang et al., 2005). In addition, an analysis of the mineral composition of $PM_{2.5}$ pollutants indicates that the major crustal elements Mg and Si are almost 1.40 to 2.24 times more abundant in Beijing than in Shanghai (Yang et al., 2005). For studies based on remote sensing, ground level fine particulate matter and aerosol optical depth (AOD) data are derived from moderate resolution satellite data, such as Moderate Resolution Imaging Spectroradiometer (MODIS) (Tian and Chen, 2010) and SeaWiFS (Vidot et al., 2007). This data are then used to estimate PM_{10} and $PM_{2.5}$. With the emergence of high-resolution data (e.g., Chinese Huanjing-1 (HJ-1) satellite and Gaofen-1 (GF-1) wide-field view (WFV) satellite) in recent years, high-resolution AOD data can be retrieved to increase the accuracy of urban air quality monitoring (Li et al., 2012; Bao et al., 2016).

Based on the two sources of $PM_{2.5}$ data and the impact of various factors on $PM_{2.5}$ concentration, most researchers have focused on meteorological factors (e.g., temperature, humidity, and wind speed) and two-dimensional surface morphology (Beckett et al., 2000; Hien et al., 2002; Moore et al., 2007; Xian, 2007; Jim and Chen, 2008; Tai et al., 2010). Tai et al. (2010) applied a multiple linear regression (MLR) model to study the correlations of total $PM_{2.5}$ and its components with meteorological variables in the United States. The research suggested that an MLR model can explain up to 50% of the $PM_{2.5}$ variability with temperature, relative humidity (RH), and precipitation. Xian (2007) investgated two-dimensional surface morphology (land use and land cover) impacts in the Las Vegas region and suggested that $PM_{2.5}$ was apparently impacted by the impervious surface area (ISA) in a 1 km grid and was weakly impacted by the urban vegetation canopies within 1 km and 2 km grids. Beckett demonstrated that urban tree species could impact particulate pollution, and a similar conclusion had been proposed by Jim for Guangzhou, China (Beckett et al., 2000; Jim and Chen, 2008). Moreover, Escobedo evaluated the spatial heterogeneity of urban forest influences on air pollution removal at a sub-regional scale and suggested that air pollution removal per square meter of tree cover was greatest in the low socioeconomic sub-region (Escobedo and Nowak, 2009). Although a variety of factors have been explored in previous studies, the scale of two-dimensional data may introduce uncertainty (Xian, 2007; Mansfield et al., 2015; Xu et al., 2016).

In recent years, the impact of urban morphology on meteorology and public transportation in various cities had been studied (Liu et al., 2014). Moreover, the relationship between urban two-dimensional (2D) morphology and air pollution had been widely examined in China (Fan et al., 2018; Liu et al., 2018; Shi et al., 2019). Because ventilation channels can accelerate atmospheric circulation and help diffuse air pollution, several cities in China have presented designs for ventilation channels from urban three-dimensional (3D) morphologies perspective to relieve air pollution (Xinhua News Agency, 2016). During the past of urban planning, 3D morphologies are considered an inconvenient factor, especially in megacities (Handayanto et al., 2017). Urban 3D morphology may be a key factor that impacts air pollution and even $PM_{2.5}$. However, investigations of the impacts on $PM_{2.5}$ concentrations still ignore urban three-dimensional (3D) characteristics.

Beijing experienced severe air pollution in 2013. Exploring the impact of urban 3D morphology on $PM_{2.5}$

concentration during this period will objectively reveal scientific laws. The findings can provide novel insights for government control of $PM_{2.5}$ pollution from the perspective of urban 3D morphology. In this paper, 39 $PM_{2.5}$ monitoring sites in Beijing of China with urban 3D morphologies and automatic $PM_{2.5}$ monitoring data were selected. The meteorological condition and public transportation factors were eliminated by analyzing the temporal patterns of $PM_{2.5}$ concentrations. We then established urban 3D morphology indices and comprehensively investigated the spatial-temporal correlations between the urban 3D morphology indices and $PM_{2.5}$ concentrations to evaluate the impacts of urban 3D morphology on $PM_{2.5}$ concentrations.

2 Materials and Methods

2.1 Study area

The study area covers the whole Beijing of China, which consists of 14 districts and 2 counties. The total area is 16 410.54 km^2 and the built-up area has reached 1289.30 km^2. Beijing experienced the most serious air pollution in 2013 and $PM_{2.5}$ was the main pollutant (Ji et al., 2014). To monitor and control the $PM_{2.5}$, government agencies had invested to build a large number of $PM_{2.5}$ monitoring sites. The Fig. 1 shows the spatial distribution of 39 $PM_{2.5}$ monitoring sites. These sites are distributed from the urban central to suburbs. The descriptions of all sites are summarized in Table 1. The urban 3D morphology of Shangdianzi, Changping_2, Chaoyang, Shunyi_2, and Baolian are shown in Fig. 2.

2.2 Data sources and data processing

Among the 39 $PM_{2.5}$ monitoring sites, 34 $PM_{2.5}$ monitoring sites belong to the Environmental Protection Agency (EPA), while 5 $PM_{2.5}$ monitoring sites (Shangdianzi, Changping_2, Chaoyang, Shunyi_2 and Baolian) belong to the Beijing Meteorological Administration (BMA). Meteorological data of EPA site were acquired from the closest weather stations and the meteorological data of BMA site were recorded with $PM_{2.5}$ concentration. The $PM_{2.5}$ concentrations at monitoring sites were collected for the period starting at 0:00 on 2013-01-01 to 24:00 on 2013-12-31. The high-resolution remote

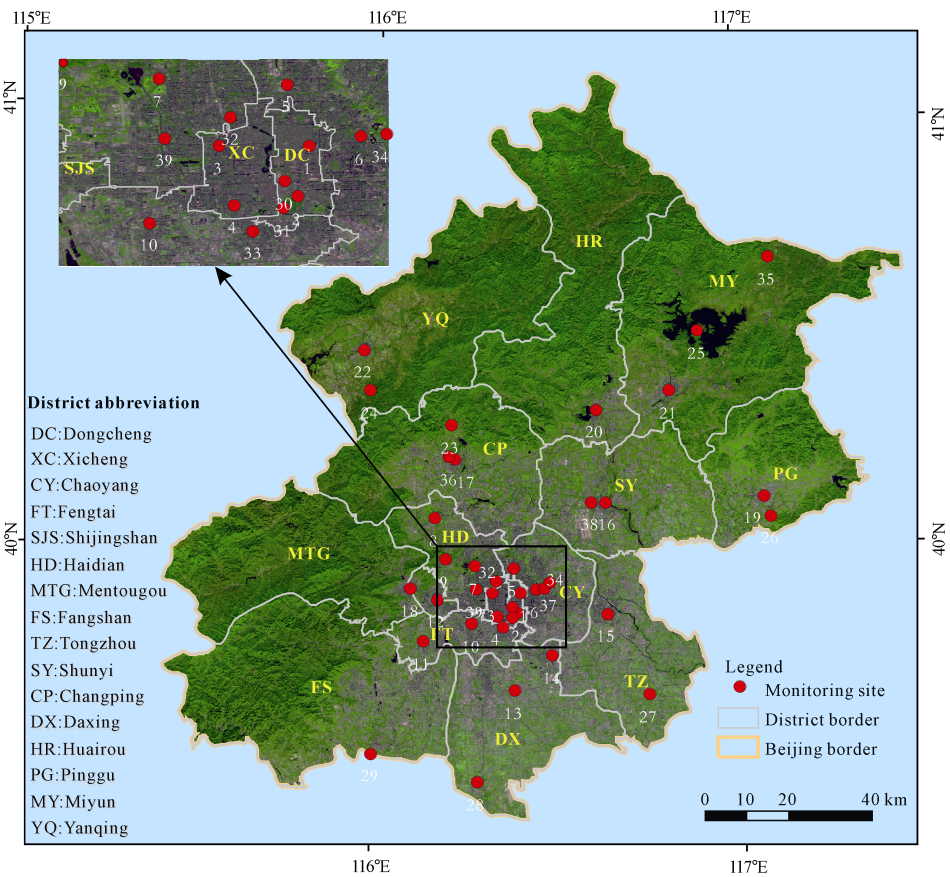

Fig. 1 Distribution of the 39 $PM_{2.5}$ monitoring sites in Beijing, China. (The number of the sites corresponds to the site name in Table 1)

Table 1 Description of the 39 $PM_{2.5}$ monitoring sites in the study area

No.	Name	No.	Name	No.	Name	No.	Name
1	Dongsi	11	Yungang	21	Miyun	31	Yongding Gate Avenue
2	Temple of Heaven	12	Gucheng	22	Yanqing	32	Xizhimen north
3	Guanyuan	13	Daxing	23	Dingling	33	Nansanhuan
4	West Wanshou	14	Yizhuang	24	Badaling	34	Dongsihuan
5	Olympic Sports Center	15	Tongzhou	25	Miyun Reservoir	35	Shangdianzi
6	Agriculture exhibition center	16	Shunyi_1	26	Donggao Village	36	Changping_2
7	Wanliu	17	Changping_1	27	Youngledian	37	Chaoyang
8	Northern New Area	18	Mentougou	28	Yufa	38	Shunyi_2
9	Botanic Garden	19	Pinggu	29	Liuli River	39	Baolian
10	Fengtai garden	20	Huairou	30	Qianmen		

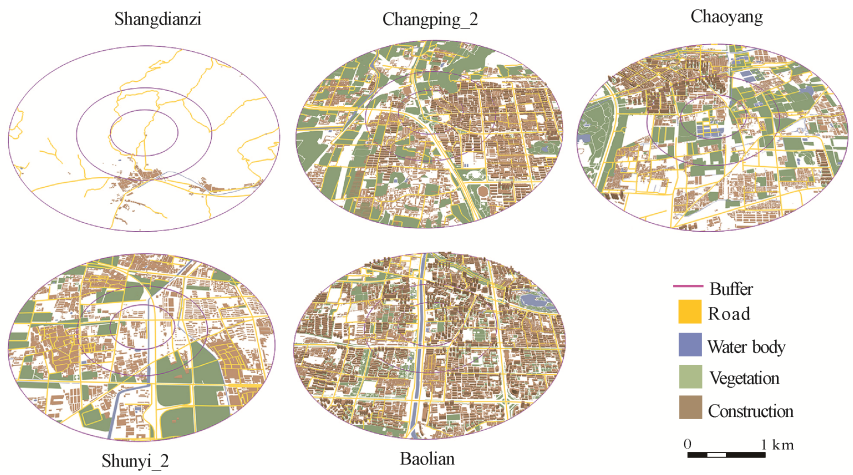

Fig. 2 The urban 3D morphology of five typical sites in Beijing, China. (The three circles correspond to 500 m, 1000 m and 2000 m buffers from inside to outside)

sensing images used in this research are collected by Quickbird, and the acquisition date was 2010-08-03. Because the land use around $PM_{2.5}$ monitoring sites were restricted by urban planning, the urban 3D morphology had slightly changed from 2010 to 2013. Therefore, the effect of period different between $PM_{2.5}$ monitoring sites data and urban 3D morphology could be ignored. The image processing includes geometric correction, image fusion and image mosaic. According to the China standard of urban land use and planning classification, the four types of urban morphology (road, water body, construction and vegetation) were extracted from high resolution Quickbird images via artificial visual discrimination with eCognition software platform. Those data were stored as vector types. The height of construction multiplied by the number of layers on each floor yielded a statistical average height of 3 m. The construction data were collected from the 2010 Beijing Civil Affairs Bureau (BCAB) field survey results.

2.3 Method

2.3.1 Underlying principles and research flow

The urban $PM_{2.5}$ concentrations are influenced by various factors (Hochadel et al., 2006; Xian, 2007; Tai et al., 2010). Meteorological conditions affect the diffusion of $PM_{2.5}$ pollutants, and public transportation is an important source of $PM_{2.5}$ pollutants (Brauer et al., 2003; Wen et al., 2018). Moreover, urban 3D morphology impacts the meteorological condition and public transportation (Collier 2006; Liu et al., 2014). Therefore, three main factors are selected for this analysis: meteorological condition, public transportation, and urban 3D morphology.

The experiment flow of this research is shown in Fig. 3. First, the meteorological data and $PM_{2.5}$ concentration data are acquired via ground monitoring sites. The impact of meteorological condition on $PM_{2.5}$ concentrations can be analyzed from two perspectives: the relationships between average wind speed and the daily and

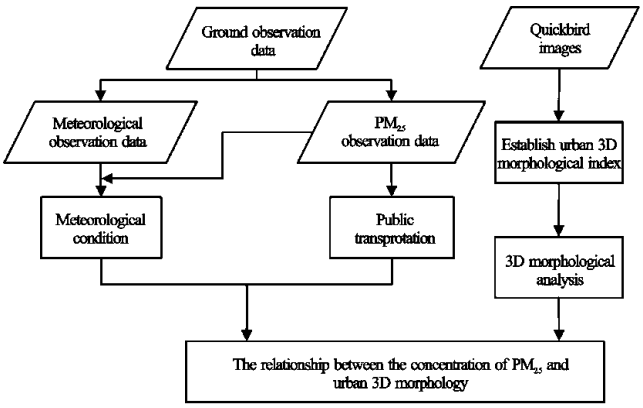

Fig. 3 Flow chart of the research

weekly $PM_{2.5}$ concentrations as well as between average wind speed and the monthly variation of $PM_{2.5}$ concentrations. Moreover, the effects of public transportation factors on the $PM_{2.5}$ concentrations will be revealed by an analysis of the weekly and daily variations of $PM_{2.5}$ concentrations. Secondly, the impacts of the meteorological condition and public transportation on the $PM_{2.5}$ concentrations can be eliminated by averaging the $PM_{2.5}$ concentrations over different time scales. This can highlight the differences in $PM_{2.5}$ concentrations due to urban 3D morphology. Finally, through extracting and analyzing urban 3D morphology indices based on high resolution images, the relationship between the urban 3D morphology and $PM_{2.5}$ concentrations at various spatial scales can be evaluated using a spatial-correlation method.

2.3.2 Establishing 3D morphological indicators

Urban 3D morphology is affected by the natural, social, economic, and urban environments. It reflects the comprehensive properties of the city, and it affects the distribution and transmission of a city's material, energy, and information (Liu et al., 2014). In this study, we establish 3D morphological indicators of the morphology of four land uses, roads, water body, construction, and vegetation. Moreover, density, height, and structural indicators are considered to extract the 3D urban morphology. The formulations for each indicator are shown in Table 2.

2.3.3 Statistics and analysis

To eliminate the instrumental and human causes of data errors, $PM_{2.5}$ automatic monitoring data throughout the year are filtered according to the China Ambient Air Quality Standards (CAAQI). The time scale for the meteorological condition changes is yearly variation, and the time scales for public transportation are weekly variation and hourly variation. Therefore, the monthly, weekly, and hourly of $PM_{2.5}$ concentrations will be calculated by averaging the effective data. To explore the correlation between $PM_{2.5}$ concentrations and wind speed, the monthly average wind speed is also included in the analysis.

To explore the potential relation between urban morphology and $PM_{2.5}$ concentrations, different scale buffers (500 m, 1000 m, and 2000 m radius circular) centered on each site are generated (Xian, 2007; Xu et al., 2016) and the urban 3D morphological indicators are calculated for each buffer. The results are shown in Fig. 4. For each buffer, the correlations between the $PM_{2.5}$ concentrations and the urban 3D morphological indices were analyzed via monthly, weekly, and daily variation. The Pearson correlation coefficient is calculated by Equation (1):

$$r=\frac{N\sum_{i=1}^{N}x_i y_i-\sum_{i=1}^{N}x_i\sum_{i=1}^{N}y_i}{\sqrt{N\sum_{i=1}^{N}x_i^2-\left(\sum_{i=1}^{N}x_i^2\right)^2}\sqrt{N\sum_{i=1}^{N}y_i^2-\left(\sum_{i=1}^{N}y_i\right)^2}} \quad (1)$$

where r is the Pearson correlation coefficient and x_i is the $PM_{2.5}$ concentrations for the ith site. y_i is the urban 3D morphology index value for the i-th site, and N is the total number of sites. To investigate the significance levels of the correlations, confidence levels of 95% ($P < 0.05$) or 99% ($P < 0.01$) are calculated using a one-sided test.

3 Results

3.1 Urban 3D morphology at different spatial scales

The $PM_{2.5}$ monitoring sites are located in regions with different urban 3D morphology. Using the ArcGIS software platform, urban 3D morphology indices are calculated according to the definition of each index in the three buffers. These results are shown in Fig. 4. There was little variation in road length density (RLD) and road area density (RAD) along the gradient from the city center to suburbs is small. However, the RLD and RAD in some typical sites, such as Botanic Garden, Liuli River, and Shangdianzi, are lower than in other sites. The water area density and water fragmentation in city center is low, but these indices are high in suburbs

Table 2 Urban 3D morphological indicators definition

Feature indicator	Indicator name	Expression	Definition
Density Features	Road Length Density	$RLD = \sum_{i=1}^{n} L_i / S$	Refers to the area ratio of the length of all roads, where L_i is the length of road section i, n is the number of roads, and S is the area of the range
	Road Area Density	$RAD = \sum_{i=1}^{n} B_i / S$	Refers to the area ratio of the area of all roads, where B_i is the area of road section i, n is the number of roads, and S is the area of the range
	Construction Area Density	$CAD = \sum_{i=1}^{n} A_i / S$	Refers to the area ratio of the area of all construction sites, where A_i is the area of construction section i, n is the number of construction sites, and S is the area of the range
	Construction Height Density	$CHD = \sum_{i=1}^{n} H_i / S$	Refers to the area ratio of the height of all construction sites, where H_i is the height of construction section i, n is the number of construction sites, and S is the area of the range
	Construction Volume Density	$CVD = \sum_{i=1}^{n} V_i / S$	Refers to the area ratio of the volume of all construction sites (volume = construction area × construction height), where V_i is the volume of construction site i, n is the number of constructions, and S is the area of the range
	Water Area Density	$WAD = \sum_{i=1}^{n} W_i / S$	Refers to the area ratio of the area of all water, where W_i is the area of water body i, n is the number of water, and S is the area of the range
	Vegetation Area Density	$VAD = \sum_{i=1}^{n} C_i / S$	Refers to the area ratio of the area of all vegetation, where C_i is the area of the vegetation section i, n is the number of vegetation sites, and S is the area of the range
Height Features Indicator	Construction Otherness	$CO = \delta / \overline{H}$	Refers to the height standard deviation (δ) ratio of the average height ($\overline{H}$) of all construction sites. It reflects the amount of scatter in the groups of construction areas
Structural Features Indicator	Water Fragmentation	$WF = \sum_{i=1}^{n} R_i / \sum_{i=1}^{n} Q_i$	Refers to the ratio of all water areas to the perimeter of all water areas, where R_i is the area of water body i, and Q_i is the perimeter of water body i
	Vegetation Fragmentation	$WF = \sum_{i=1}^{n} S_i / \sum_{i=1}^{n} T_i$	Refers to the ratio of all-vegetation area to the perimeter of all vegetation areas, where S_i is the area of vegetation section i, and T_i is the perimeter of vegetation section i

(e.g., Miyun Reservoir and Yanqing). This is because these stations are close to open water body. There was no obvious difference in construction area density from the city center to suburbs across among the three buffer sizes. However, there were significant differences in urban height morphology indices (i.e., construction height density, construction volume density, and construction otherness) from city center to suburbs. These differences were especially pronounced for construction otherness. Vegetation area density and vegetation fragmentation are low in the city center, but they are high in the suburbs. The morphology indices related to roads and construction decrease along the gradient from the city center to the suburbs, while the morphology indices related to water body and vegetation increase with distance from the city center.

3.2 Impact of meteorological conditions and public transportation on $PM_{2.5}$ concentrations

3.2.1 Impact of meteorological conditions on $PM_{2.5}$ concentrations

Meteorological conditions are an important factor for the aggregation and diffusion of $PM_{2.5}$ (Westervelt et al., 2016). The variations of monthly $PM_{2.5}$ concentrations in response to wind speeds and temperature are shown in Fig. 5. Fig. 5a shows the spatial variations in monthly $PM_{2.5}$ concentrations. There are significant heterogeneities in the $PM_{2.5}$ concentrations among the 39 $PM_{2.5}$ monitoring sites and the high concentration monitoring sites are located in the center and southeast of Beijing. The Shangdianzi site is located in the suburbs, and the vegetation coverage is high. The $PM_{2.5}$ concentrations at the Shangdianzi site are lowest. Dongsihuan, Nansanhuan, and Qianmen are located in a transportation hub. The $PM_{2.5}$ concentration variations for those three sites are high. The BL, Olympic sports center, and agriculture exhibition center are located in the city center, where photochemical reactions easily occur in the summer (Huang et al., 2012). Therefore, the $PM_{2.5}$ concentrations are high at these sites.

The amplitudes of the $PM_{2.5}$ monthly average concentrations are high and exhibit two 'peak-valley' forms (Fig. 5b). There is a significant peak in January with a concentration of 169.51 μg/m^3. This far exceeds the Ambient Air Quality Standards (AAQS) (Hu et al., 2013). The peaks in January are due to the increased stability of the atmosphere with low wind speeds (Li et al., 2009). The $PM_{2.5}$ concentrations are low during spring and summer, whereas they fluctuate from September to December. The possible explanations are as follows. 1) The wind speed is high from March to June in Beijing and the deciduous vegetation growth is able

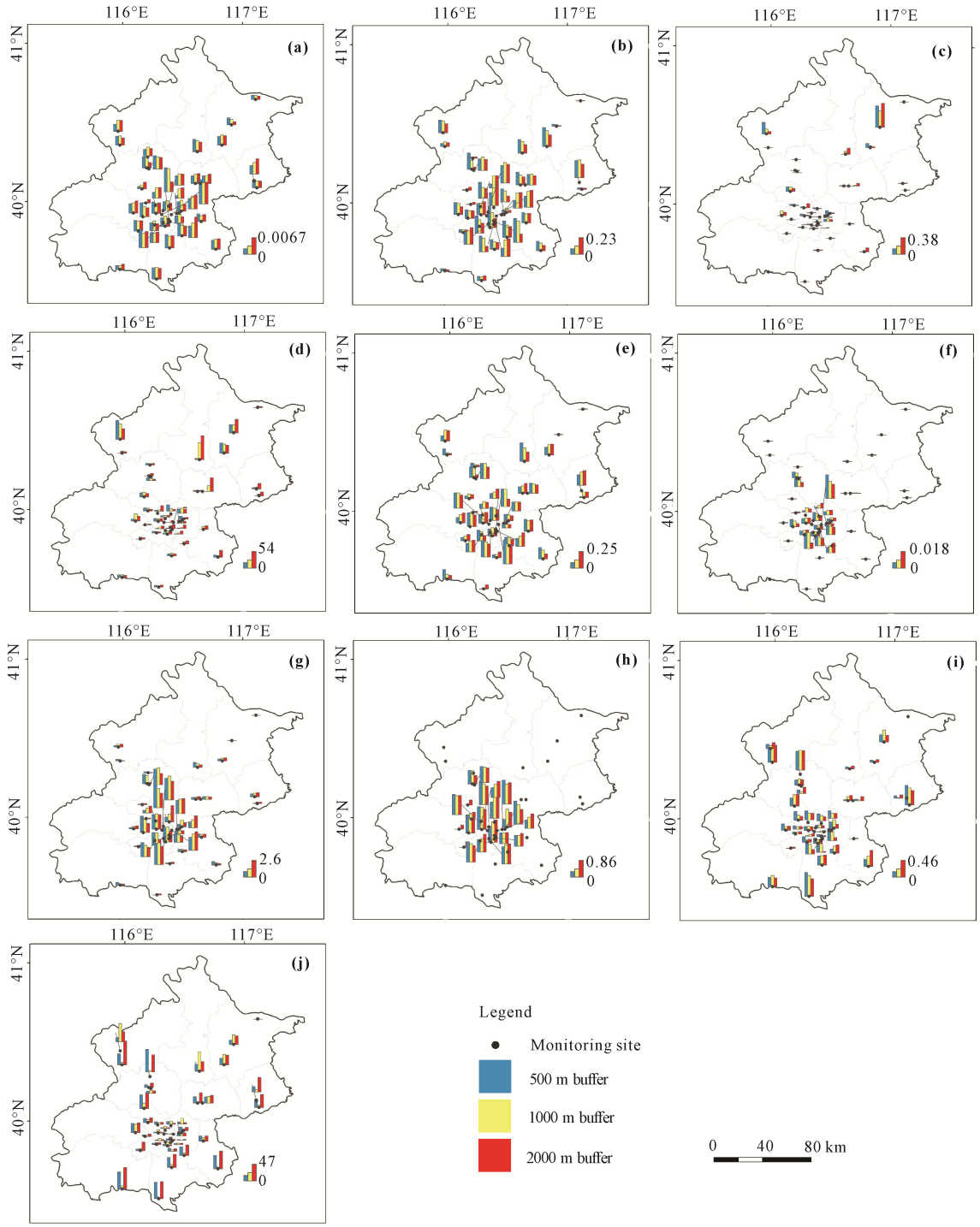

Fig. 4 Urban morphology indices for each site. (a) Road Length Density (RLD); (b) Road Area Density (RAD); (c) Water Area Density (WAD); (d) Water Fragmentation (WF); (e) Construction Area Density (CAD); (f) Construction Height Density (CHD); (g) Construction Volume Density (CVD); (h) Construction Otherness (CO); (i) Vegetation Area Density (VAD); and (j) Vegetation Fragmentation (VF) (The 500 m, 1000 m and 2000 m correspond to the three buffers)

to absorb and hold $PM_{2.5}$ (Jim and Chen, 2008). 2) The low $PM_{2.5}$ concentrations in summer may have been due to increased precipitation from June to August (Filonchyk et al., 2016). 3) The low concentrations in autumn and winter from September to December may have been associated with regional meteorological conditions, such

as the wind directions changing from southeast to northwest (Song et al., 2012).

The monthly averaged wind speeds and temperature are also shown in Fig. 5b. There is an insignificant negative correlation between the $PM_{2.5}$ concentrations and wind speeds. The peaks of the $PM_{2.5}$ concentrations correspond to the local minima of wind speeds in January, June, and October. However, the local minimum of $PM_{2.5}$ concentrations in April corresponds to valley local maximum in wind speeds. This result indicates that faster wind speeds increase air circulation which could reduce $PM_{2.5}$ concentrations and improve air quality (Lu and Fang, 2002; Wen et al., 2018). Moreover, there is no strong correlation between temperature and $PM_{2.5}$ concentrations, which indicates that the temperature is not a key factor affecting $PM_{2.5}$ concentrations.

3.2.2 Impact of public transportation factors on $PM_{2.5}$ concentrations

The statistical weekly averages (Monday to Sunday) of $PM_{2.5}$ concentrations among the 39 $PM_{2.5}$ monitoring sites throughout 2013 are shown in Fig. 6a. The $PM_{2.5}$ concentrations ranged from 74.05 to 95.99 μg/m^3. The $PM_{2.5}$ concentrations show decreased trend from Monday to Friday and increased from Saturday to Sunday. The reason for this pattern may be related to the public traffic intensity change.

The hourly averages of the $PM_{2.5}$ concentration among the 39 $PM_{2.5}$ monitoring sites throughout the year are shown in Fig. 6b. The $PM_{2.5}$ concentrations show significant increases from 5:00 to 8:00 during the rush hours. During the typical working hours (9:00 to 14:00), the $PM_{2.5}$ concentrations decrease from 95.42 to

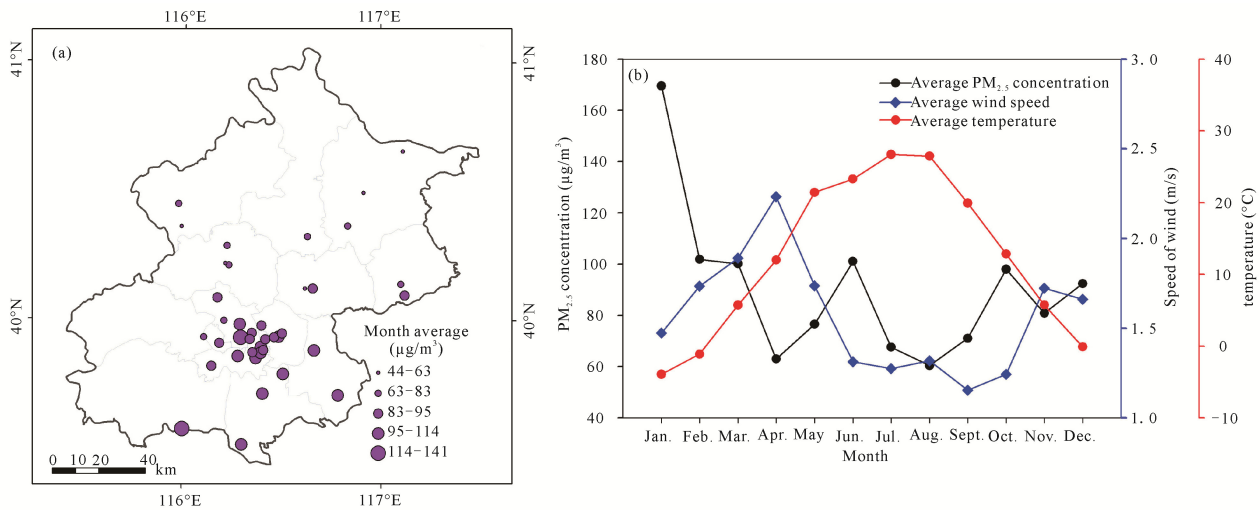

Fig. 5 Change of $PM_{2.5}$ concentrations with wind speed and temperature. (a) Spatial pattern of $PM_{2.5}$ monthly concentrations. (b) Monthly variations of $PM_{2.5}$ concentrations, wind speeds and temperature

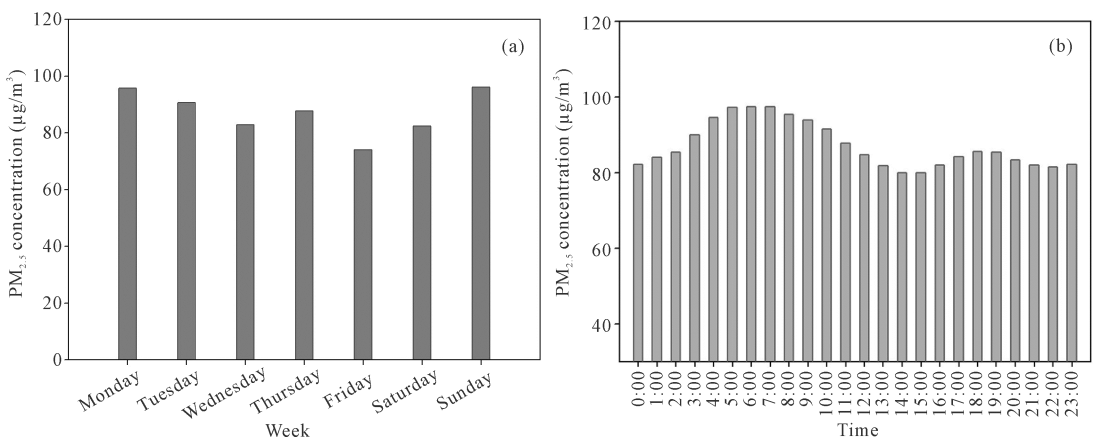

Fig. 6 The weekly (a) and hourly (b) $PM_{2.5}$ concentrations in Beijing, China

79.99 μg/m^3. The $PM_{2.5}$ concentrations increase after work from 16:00 until 19:00, and they reach a maximum of 85.37 μg/m^3. The $PM_{2.5}$ concentrations begin to decrease at 20:00, which corresponds to typical sleep periods in the population.

3.3 Relations between $PM_{2.5}$ concentrations and urban 3D morphology

The monthly average $PM_{2.5}$ concentrations for the 39 $PM_{2.5}$ monitoring sites during the 2013 were calculated to eliminate the effects of the meteorological factors on the $PM_{2.5}$ concentrations, and the $PM_{2.5}$ weekly and daily average concentrations are calculated to eliminate the effects of the public transportation factors. Furthermore, to explore the correlations between urban 3D morphology and $PM_{2.5}$ concentrations, ten urban 3D morphology indices are calculated at different scales (500 m, 1000 m, and 2000 m buffers).

Scatter graphs of the road morphology indices and $PM_{2.5}$ concentrations are shown in Fig. 7. The correlation coefficients between RLD and the monthly, weekly, and daily $PM_{2.5}$ concentrations in the 2000 m buffer are 0.243, 0.237 and 0.238, respectively, and those coefficients increase with the expansion of the buffer scale. This finding indicates that RLD has a greater impact on the $PM_{2.5}$ concentrations at the larger scales, but that pattern is inconsistent at different time scales. The correlations between RAD and $PM_{2.5}$ concentrations are significant at the 2000 m buffer scale. The correlation coefficients increase with the expansion of the buffer scale. In the 500 m buffer, the correlation coefficients between RAD and the monthly, weekly, and daily $PM_{2.5}$ concentrations are 0.184, 0.173, and 0.173, respectively. These values increase to 0.271, 0.274, and 0.275, respectively at the 2000 m buffer scale. These results indicate that higher values in road morphology indices entail higher $PM_{2.5}$ concentrations.

The correlation coefficients for the two water body morphological indices and the $PM_{2.5}$ concentrations exhibited large variations at different spatial scales (Fig. 8).

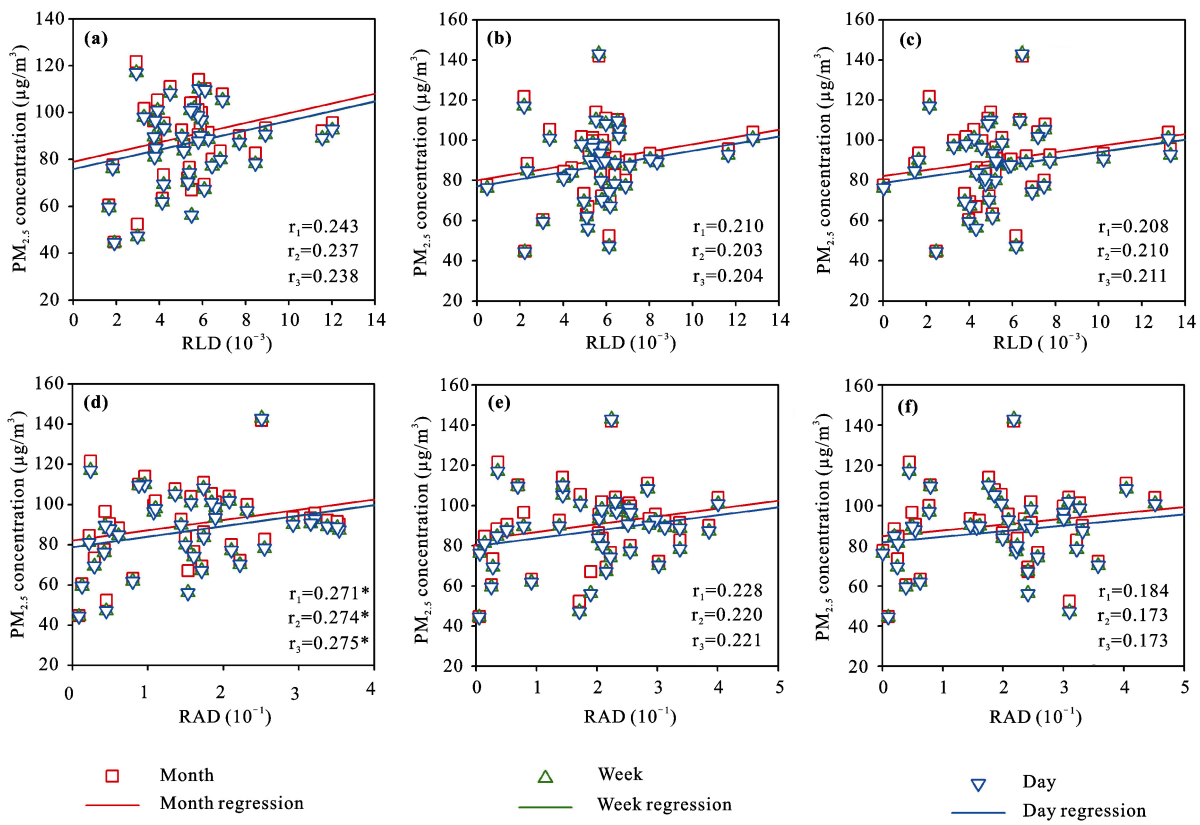

Fig. 7 Correlations between the $PM_{2.5}$ concentrations and the road morphology indices. Panels (a), (b), and (c) are scatterplots of the road length density (RLD) indices and $PM_{2.5}$ concentrations at the 2000 m, 1000 m and 500 m buffer scales, respectively. Panels (d), (e), and (f) are scatterplots of the road area density (RAD) indices and $PM_{2.5}$ concentrations at the 2000 m, 1000 m, and 500 m buffer scales, respectively. The r_1, r_2, r_3 correspond to coefficients of the month relation, week relation and day relation, respectively. * $P < 0.05$

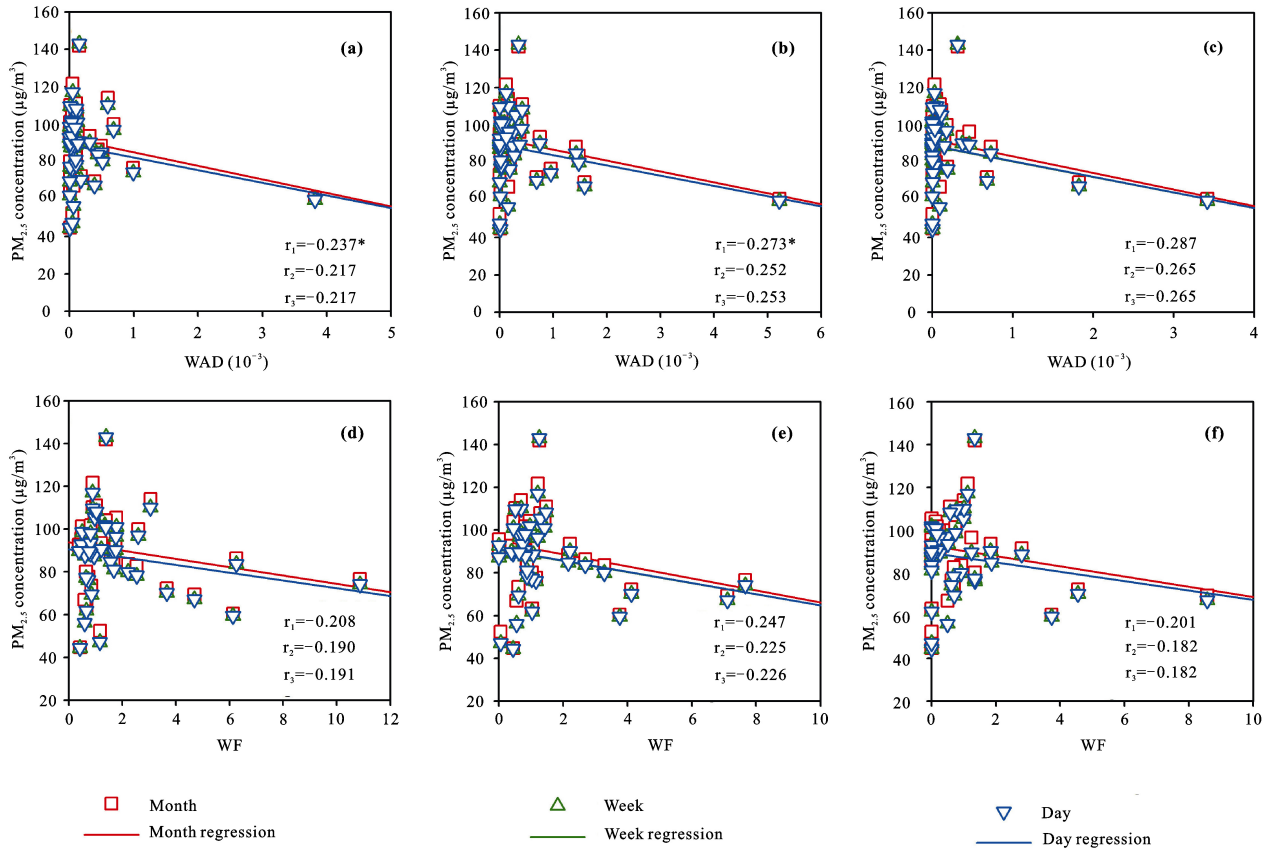

Fig. 8 Correlations between the $PM_{2.5}$ concentrations and the water indices. Panels (a), (b), and (c) are scatterplots of the water area density (WAD) index and $PM_{2.5}$ concentrations at 2000 m, 1000 m and 500 m buffers, respectively. Panels (d), (e), and (f) are scatterplots of the water fragmentation (WF) index and $PM_{2.5}$ concentrations at the 2000 m, 1000 m, and 500 m buffer scales, respectively. The r_1, r_2, r_3 correspond to the coefficients of month relation, week relation and day relation, respectively. * $P < 0.05$

The correlation between WAD and $PM_{2.5}$ concentrations in the 500 m buffer are low, whereas the correlations are high for the 1000 m and 2000 m buffer scales. These results demonstrate that the correlations between WAD and $PM_{2.5}$ concentrations are high at small scales. The correlations between WF and the $PM_{2.5}$ concentrations are highest in the 1000 m buffer. The WF exhibited higher correlations with $PM_{2.5}$ concentrations than WAD. This demonstrates that WAD is more sensitive than WF to the $PM_{2.5}$ concentrations. The correlation trends between water body morphology indices and $PM_{2.5}$ concentrations indicate that water areas have a negative impact on the $PM_{2.5}$ concentrations.

The construction indices are the main components of the urban 3D morphology indices, and their correlation results are shown in Fig. 9. The correlations between four construction indices and the $PM_{2.5}$ concentrations are positive across the three buffers scales. As to four construction indices, the correlations are highest at the 2000 m buffer scale. The coefficient of height dimension indices (CHD, CVD, and CO) with $PM_{2.5}$ show significant correlation at 2000 m buffer, which suggests that the urban construction height can impact the $PM_{2.5}$ concentrations.

The results of the correlation analysis between the vegetation indices and the $PM_{2.5}$ concentration are shown in Fig. 10. The correlations between VAD and the $PM_{2.5}$ concentrations at the three buffers scales are slightly positive. The correlations between VF and the $PM_{2.5}$ concentrations are positive at the 500 m buffer scale, however, the correlations at the 1000 m and 2000 m buffer scales are negative. The fragmentation degree of vegetation can help reduce the $PM_{2.5}$ concentrations, but this effect is greater at larger buffer scales.

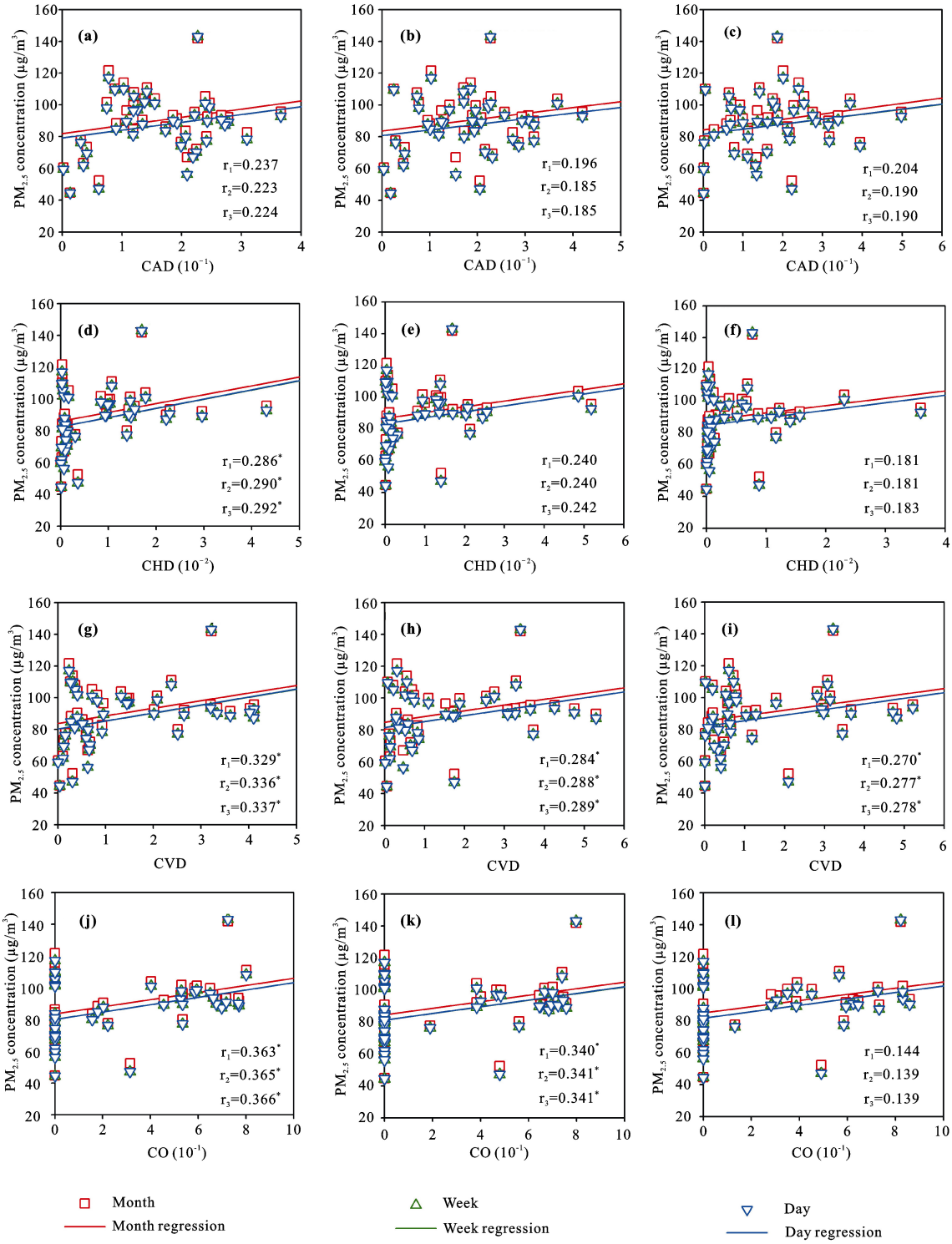

Fig. 9 Correlations between the $PM_{2.5}$ concentrations and construction indices. Panels (a), (b), and (c) show scatterplots of the construction area Density (CAD) index and $PM_{2.5}$ concentrations for the 2000 m, 1000 m and 500 m buffer scales, respectively. Panels (d), (e), and (f) show scatterplots of the construction height density (CHD) index and $PM_{2.5}$ concentrations at the 2000 m, 1000 m, and 500 m buffer scales, respectively. Panels (g), (h), and (i) show scatterplots of the construction volume density (CVD) index and $PM_{2.5}$ concentrations for the 2000 m, 1000 m, and 500 m buffer scales. The panels (j), (k), and (l) show scatterplots for the construction otherness (CO) index and $PM_{2.5}$ concentrations at the 2000 m, 1000 m, and 500 m buffer scales, respectively. The r_1, r_2, r_3 correspond to the coefficients of month relation, week relation and day relation, respectively. * $P < 0.05$

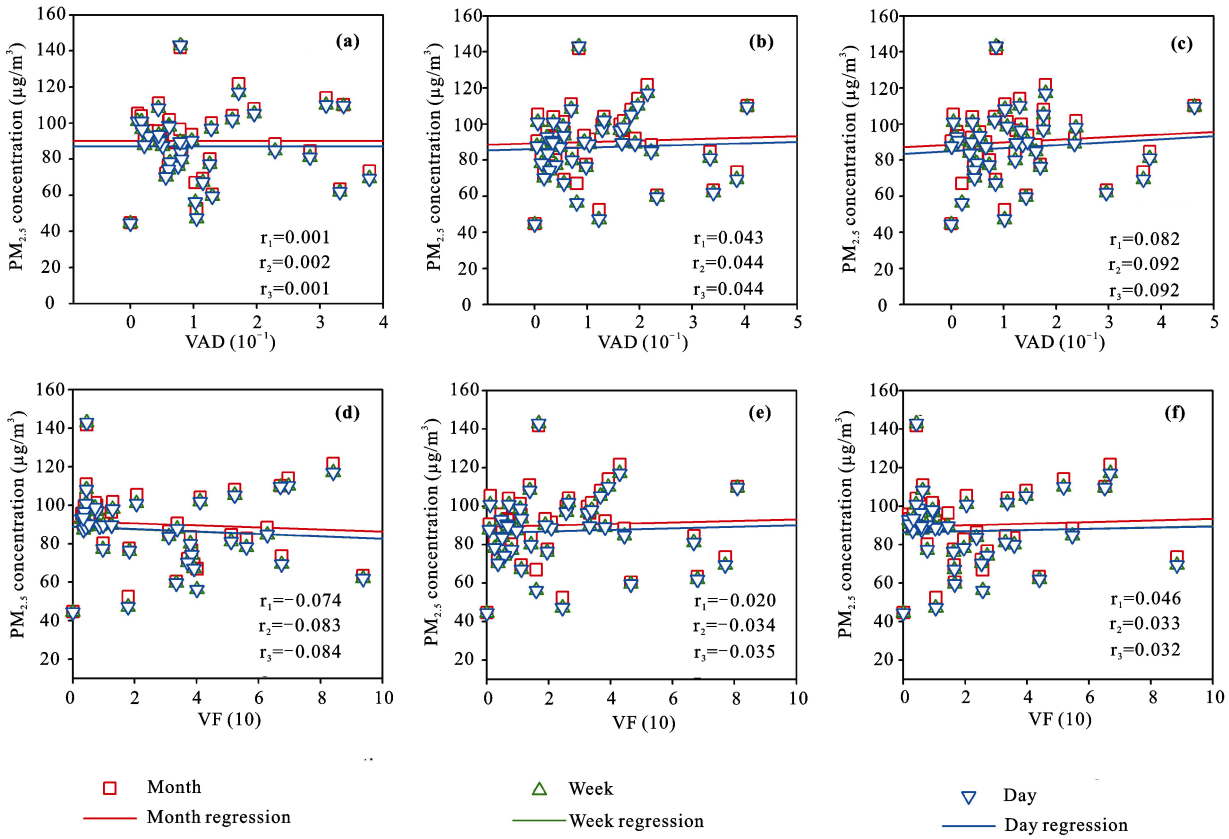

Fig. 10 Correlations between $PM_{2.5}$ concentrations and vegetation indices. Panels (a), (b), and (c) show scatterplots of the vegetation area density (VAD) index and $PM_{2.5}$ concentrations for the 2000 m, 1000 m and 500 m buffer scales, respectively. Panels (d), (e), and (f) show scatterplots of the vegetation fragmentation (VF) index and $PM_{2.5}$ concentrations for the 2000 m, 1000 m, and 500 m buffer scales, respectively. The r_1, r_2, r_3 correspond to the coefficients of month relation, week relation and day relation, respectively

4 Discussion

The risks of severe air pollution have been increasingly highlighted over the past decades (Zhang and Cao, 2015) and a series of studies have explored the causes of $PM_{2.5}$ (Yang et al., 2005; Moore et al., 2007; Tai et al., 2010). This paper aims to investigate the impact of urban 3D morphology on $PM_{2.5}$ concentrations. Aspects of three factors, meteorological conditions, public transportation, and urban 3D morphology, have been extensively discussed. However, urban 3D morphology has an obvious impact on other the two factors.

Before analyzing the effects of urban morphology on $PM_{2.5}$ concentrations, the impacts of meteorological conditions and public transportation on $PM_{2.5}$ concentrations were analyzed using monthly, weekly, and hourly $PM_{2.5}$ monitoring sites data. It should be noted that only one meteorological condition factor, wind speed, was collected to discuss its correlations with $PM_{2.5}$ concentrations. This is because wind speed is a commonly used sensitivity factor that impacts $PM_{2.5}$ concentrations, and this influence is sometimes even decisive in Beijing (Yin et al., 2016). In addition, the patterns of weekly and hourly $PM_{2.5}$ concentrations related to public transportation are determined. The results can demonstrate the impacts of public transportation on $PM_{2.5}$ concentrations, and these results are consistent with those of a previous study (Yin et al., 2016).

Ten urban 3D morphological indicators were then are calculated for 39 $PM_{2.5}$ monitoring sites at different buffer scales. In 2013, there were 39 $PM_{2.5}$ monitoring sites in Beijing. The annual dataset of $PM_{2.5}$ concentrations collected at these sites were utilized for this study. Those sites located in different functional zones that range from urban center to suburbs. Therefore, those sites are representative for spatial analysis. Surely, if there are denser stations with long-term $PM_{2.5}$ concentration monitoring sites data, more statistical samples

will be obtained to analyze correlations between urban 3D morphological indices and $PM_{2.5}$ concentrations. Therefore, the correlation uncertainties can be further reduced.

The correlations between $PM_{2.5}$ concentrations and urban 3D morphology are summarized in Table 3. The data suggest that RLD, RAD, CAD, CHD, CVD, CO, and VAD have positive impacts on the $PM_{2.5}$ concentrations, whereas WAD, WF, and VF (except at the 500 m buffer scale) have negative impacts on the $PM_{2.5}$ concentrations.

From the perspective of source apportionment, road emissions are among the major sources of $PM_{2.5}$ pollution (Song et al., 2012; Hu et al., 2013). The impact of public transportation and road morphology on $PM_{2.5}$ concentrations are further confirmed from spatial-temporal perspective. Through in-depth analysis of traffic factors, it is helpful to build more universe models for larger spatial scale simulation (Brauer et al., 2003). Water body can affect the local relative humidity, and relative humidity is one of meteorological factor that affects the formation of particulate matter (Hien et al., 2002). Based on the correlation analyses, $PM_{2.5}$ concentrations are more susceptible to impacts from water transpiration areas than impacts from spatial structure. Previous studies using land use modeling to predict $PM_{2.5}$ concentrations demonstrate that construction area is a key factor that impacts $PM_{2.5}$ concentrations (Moore et al., 2007; Xian, 2007). The correlation coefficients between the $PM_{2.5}$ concentrations and urban height dimension indices (CHD, CVD, and CO) are significant at the 2000 m buffer scale, and a positive correlation can be determined. Generally, a rational distribution of urban heights can help improve air circulation and local micro-climates within the city. The construction of artificial ventilation corridors via urban planning and the establishment of measures that protect a city's natural ventilation corridors can effectively enhance air circulation, thereby reducing concentrations of $PM_{2.5}$ pollutants (Xin et al., 2012). The effect of these measures can be especially pronounced in dense urban areas with tall built up areas. Vegetation can help improve regional ecological environments and trap particulate matter pollutants (Jim and Chen, 2008). Moreover, this effect is affected by wind and tree species (Beckett et al., 2000). Our study also found that vegetation structure can negatively impact $PM_{2.5}$ concentration.

This study investigates the impacts of urban 3D morphology on the $PM_{2.5}$ concentrations and, the impacts of 3D morphology are concisely analyzed by eliminating meteorological and public transportation factors. Our findings provide important idea that can help authorities control air pollution via urban planning.

5 Conclusions

Urban morphology may impact air pollution concentration by changing atmospheric circulation. This paper investigated the impact of urban 3D morphology on $PM_{2.5}$ concentrations in 2013 of Beijing, China. The meteorological condition and public transportation factors were eliminated and the spatial-temporal correlations between the urban 3D morphology indices and $PM_{2.5}$ concentrations were comprehensively analyzed. The conclusions are as follows:

1) The monthly $PM_{2.5}$ concentration variations are primarily affected by the meteorological conditions and are negatively correlated with wind speed. The weekly and hourly $PM_{2.5}$ concentration variations are associated with public transportation. The $PM_{2.5}$ concentrations increase during the weekends and significant increase during commute times.

2) Correlation results suggest that construction indices and road indices positively impacted $PM_{2.5}$ concentrations, whereas water indices and vegetation indices (except VF at the 500 m buffer scale) negatively impact

Table 3 The correlation trends of the ten morphology indexes for the three buffers

Index	2000 m	1000 m	500 m	Index	2000 m	1000 m	500 m
RLD	+	+	+	CHD	+	+	+
RAD	+	+	+	CVD	+	+	+
WAD	–	–	–	CO	+	+	+
WF	–	–	–	VAD	+	+	+
CAD	+	+	+	VF	–	–	+

Notes: + represents a positive correlation, and – represents a negative correlation. Meanings of abbreviations see Table 2

the $PM_{2.5}$ concentrations. The correlations between the morphology indices and $PM_{2.5}$ concentrations varied across buffer scales. The coefficient of height dimension indices with $PM_{2.5}$ suggested that the urban construction height can impact the $PM_{2.5}$ concentrations.

These results aid in developing an understanding of the impacts of $PM_{2.5}$ concentrations from the perspective of urban 3D morphology. The results have potential applications in regulating urban air pollution from the perspective of urban 3D morphology. Buffer scale is a factor that impacts correlation level, and scale issues that arise in assessing the impact of urban 3D morphology on $PM_{2.5}$ concentrations need to be addressed in the next study.

References

Bao F W, Gu X F, Cheng T H et al., 2016. High-spatial-resolution aerosol optical properties retrieval algorithm using Chinese high-resolution earth observation satellite I. *IEEE Transactions on Geoscience and Remote Sensing*, 54(9): 5544–5552. doi: 10.1109/tgrs.2016.2568246

Beckett K P, Freer P H, Taylor G, 2000. Particulate pollution capture by urban trees: effect of species and windspeed. *Global Change Biology*, 6(8): 995–1003. doi: 10.1046/j.1365-2486. 2000.00376.x

Bonyadi Z, Ehrampoush M H, Ghaneian M T et al., 2016. Cardiovascular, respiratory, and total mortality attributed to $PM_{2.5}$ in Mashhad, Iran. *Environmental Monitoring and Assessment*, 188(10): 570. doi: 10.1007/s10661-0165574–y

Brauer M, Hoek G, Van V P et al., 2003. Estimating long-term average particulate air pollution concentrations: application of traffic indicators and geographic information systems. *Epidemiology*, 14(2): 228–239. doi: 10.1097/00001648–200303000–00019

Cao C, Lee X, Liu S D et al., 2016. Urban heat islands in China enhanced by haze pollution. *Nature Communications,* 7:12509. doi: 10.1038/ncomms12509

Chen Tan, Deng Shulin, Gao Yu et al., 2017. Characterization of air pollution in urban areas of Yangtze River Delta, China. *Chinese Geographical Science*, 27(5): 836–846. doi: 10.1007/s11769-017-0900-z

Chow J C, Watson J G, Mauderly J L et al., 2006. Health effects of fine particulate air pollution: lines that connect. *Journal of the Air & Waste Management Association*, 56(10): 1368–1380. doi: 10.1080/10473289. 2006.10464585

Chuersuwan N, Turpin B J, Pietarinen C, 2000. Evaluation of time-resolved $PM_{2.5}$ data in urban/suburban areas of New Jersey. *Journal of the Air & Waste Management Association*, 50(10): 1780–1789. doi: 10.1080/10473289.2000.10464214

Collier C G, 2006. The impact of urban areas on weather. *Quarterly Journal of the Royal Meteorological Society,* 132(614): 1–25. doi: 10.1256/qj.05.199

Escobedo F J, Nowak D J, 2009. Spatial heterogeneity and air pollution removal by an urban forest. *Landscape and Urban Planning*, 90(3): 102–110. doi: 10.1016/j.landurbplan.2008.10.021

Fan C J, Tian L, Zhou L et al., 2018. Examining the impacts of urban form on air pollutant emissions: evidence from China. *Journal of Environmental Management*, 212: 405–414. doi: 10.1016/j.jenvman. 2018.02.001

Filonchyk M, Yan H W, Yang S W et al., 2016. A study of $PM_{2.5}$ and PM_{10} concentrations in the atmosphere of large cities in Gansu Province, China, in summer period. *Journal of Earth System Science,* 125(6): 1175–1187. doi: 10.1007/s12040-016-0722-x

Handayanto R T, Tripathi N K, Kim S M et al., 2017. Achieving a sustainable urban form through land use optimisation: insights from Bekasi city's land use plan (2010–2030). *Sustainability*, 9(2): 221. doi: 10.3390/su9020221

Hien P D, Bac V T, Tham H C et al., 2002. Influence of meteorological conditions on $PM_{2.5}$ and PM_{10} concentrations during the monsoon season in Hanoi, Vietnam. *Atmospheric Environment,* 36(21): 3473–3484. doi: 10.1016/s1352-2310(02)00295-9

Hochadel M, Heinrich J, Gehring U et al., 2006. Predicting long-term average concentrations of traffic-related air pollutants using GIS-based information. *Atmospheric Environment,* 40(3): 542–553. doi: 10.1016/j.atmosenv.2005.09.067

Hu M G, Jia L, Wang J F et al., 2013. Spatial and temporal characteristics of particulate matter in Beijing, China using the empirical mode decomposition method. *Science of the Total Environment*, 458–460: 70–80. doi: 10.1016/j.scitotenv.2013.04.005

Huang W, Cao J J, Tao Y B et al., 2012. Seasonal variation of chemical species associated with short-term mortality effects of $PM_{2.5}$ in Xi'an, a central city in China. *American Journal of Epidemiology,* 175(6): 556–566. doi: 10.1093/ aje/kwr342

Ji D S, Li L, Wang Y S et al., 2014. The heaviest particulate air pollution episodes occurred in northern China in January, 2013: insights gained from observation. *Atmospheric Environment,* 92: 546–556. doi: 10.1016/j.atmosenv.2014.04.048

Jim C Y, Chen W Y, 2008. Assessing the ecosystem service of air pollutant removal by urban trees in Guangzhou (China). *Journal of Environmental Management,* 88(4): 665–676. doi: 10.1016/j.jenvman. 2007.03.035

Li Xingru, Guo Xueqing, Liu Xinran et al., 2009. Distribution and sources of solvent extractable organic compounds in $PM_{2.5}$ during 2007 chinese spring festival in Beijing. *Journal of Environmental Sciences,* 21(2): 142–149. doi: 10.1016/s1001-0742(08)62242-1

Li Y J, Xue Y, He X W et al., 2012. High-resolution aerosol remote sensing retrieval over urban areas by synergetic use of HJ-1 CCD and MODIS data. *Atmospheric Environment,* 46: 173–180. doi: 10.1016/j.atmosenv.2011.10.002

Lin C Q, Li Y, Yuan Z B et al., 2015. Using satellite remote sensing data to estimate the high-resolution distribution of ground-level $PM_{2.5}$. *Remote Sensing of Environment,* 156: 117–128. doi: 10.1016/j.rse.2014. 09.015

Liu S, Fan X T, Wen Q K et al., 2014. Simulated impacts of 3D urban morphology on urban transportation in megacities: case study in Beijing. *International Journal of Digital Earth*, 7(6): 470–491. doi: 10.1080/17538947.2012.740079

Liu Y P, Wu J G, Yu D Y et al., 2018. The relationship between urban form and air pollution depends on seasonality and city size. *Environmental Science and Pollution Research*, 25(16): 15554–15567. doi: 10.1007/s11356-018-1743-6

Lu H C, Fang G C, 2002. Estimating the frequency distributions of PM_{10} and $PM_{2.5}$ by the statistics of wind speed at Sha-Lu, Taiwan. *Science of the Total Environment*, 298(1): 119–130. doi: 10.1016/s0048-9697(02)00164-x

Ma Siqi, Chen Weiwei, Zhang Shichun et al., 2017. Characteristics and cause analysis of heavy haze in Changchun City in Northeast China. *Chinese Geographical Science*, 27(6): 989–1002. doi: 10.1007/s11769-017-0922-6

Mansfield T J, Rodriguez D A, Huegy J et al., 2015. The effects of urban form on ambient air pollution and public health risk: a case study in Raleigh, North Carolina. *Risk Analysis,* 35(5): 901–918. doi: 10.1111/risa.12317

Meng R, Zhao F R, Sun K et al., 2015. Analysis of the 2014 'APEC Blue' in Beijing using more than one decade of satellite observations: lessons learned from radical emission control measures. *Remote Sensing*, 7(11): 15224–15243. doi: 10.3390/rs71115224

Miller K A, Siscovick D S, Sheppard L et al., 2007. Long-term exposure to air pollution and incidence of cardiovascular events in women. *New England Journal of Medicine,* 356(5): 447–458. doi: 10.1056/NEJMoa054409

Moore D K, Jerrett M, Mack W J et al., 2007. A land use regression model for predicting ambient fine particulate matter across Los Angeles, CA. *Journal of Environmental Monitoring,* 9(3): 246–252. doi: 10.1039/b615795e

Seltenrich N 2016. $PM_{2.5}$ exposure and intrauterine inflammation a possible mechanism for preterm and underweight birth. *Environmental Health Perspectives,* 124(10): A190. doi: 10.1289/ehp.124-190

Shi K F, Wang H, Yang Q Y et al., 2019. Exploring the relationships between urban forms and fine particulate ($PM_{2.5}$) concentration in China: a multi-perspective study. *Journal of Cleaner Production,* 231: 990–1004. doi:10.1016/j.jclepro.2019.05.317

Song S J, Wu Y, Jiang J K, et al., 2012. Chemical characteristics of size-resolved $PM_{2.5}$ at a roadside environment in Beijing, China. *Environmental Pollution,* 161: 215–221. doi: 10.1016/j.envpol.2011.10.014

Tai A P K, Mickley L J, Jacob D J 2010. Correlations between fine particulate matter ($PM_{2.5}$) and meteorological variables in the United States: implications for the sensitivity of $PM_{2.5}$ to climate change. *Atmospheric Environment,* 44(32): 3976–3984. doi: 10.1016/j.atmosenv.2010.06.060

Tao M H, Chen L F, Wang Z F et al., 2014. A study of urban pollution and haze clouds over northern China during the dusty season based on satellite and surface observations. *Atmospheric Environment,* 82: 183–192. doi: 10.1016/j.atmosenv.2013.10.010

Tian J, Chen D M, 2010. A semi-empirical model for predicting hourly ground-level fine particulate matter ($PM_{2.5}$) concentration in southern Ontario from satellite remote sensing and ground-based meteorological measurements. *Remote Sensing of Environment,* 114(2): 221–229. doi: 10.1016/j.rse.2009.09.011

Vidot J, Santer R, Ramon D, 2007. Atmospheric particulate matter (PM) estimation from SeaWiFS imagery. *Remote Sensing of Environment,* 111(1): 1–10. doi: 10.1016/j.rse.2007.03.009

Wang Q, 2013. China's citizens must act to save their environment. *Nature,* 497(7448): 159. doi: 10.1038/497159a

Wang Z F, Chen L F, Tao J H et al., 2010. Satellite-based estimation of regional particulate matter (PM) in Beijing using vertical-and-RH correcting method. *Remote Sensing of Environment,* 114(1): 50–63. doi: 10.1016/j.rse.2009.08.009

Wen Xin, Zhang Pingyu , Liu Daqian, 2018. Spatiotemporal variations and influencing factors analysis of $PM_{2.5}$ concentrations in Jilin Province, Northeast China. *Chinese Geographical Science,* 28(5): 810–822. doi: 10.1007/s11769-018-0992-0

Westervelt D M, Horowitz L W, Naik V et al., 2016. Quantifying $PM_{2.5}$ meteorology sensitivities in a global climate model. *Atmospheric Environment*, 142: 43–56. doi: 10.1016/j.atmosenv.2016.07.040

Wu J S, Yao F, Li W F et al., 2016. VIIRS-based remote sensing estimation of ground-level $PM_{2.5}$ concentrations in Beijing-Tianjin-Hebei: a spatiotemporal statistical model. *Remote Sensing of Environment*, 184: 316–328. doi: 10.1016/j.rse.2016.07.015

Xian G, 2007. Analysis of impacts of urban land use and land cover on air quality in the Las Vegas region using remote sensing information and ground observations. *International Journal of Remote Sensing,* 28(24): 5427–5445. doi: 10.1080/01431160701227653

Xin Jinyuan, Wang Yuesi, Wang Lili et al., 2012. Reductions of $PM_{2.5}$ in Beijing-Tianjin-Hebei urban agglomerations during the 2008 Olympic Games. *Advances in Atmospheric Sciences,* 29(6): 1330–1342. doi: 10.1007/s00376-012-1227-4

Xinhua News Agency, 2016. Three questions about building five urban air corridor in Beijing. Available at: http://www.xinhuanet.com//politics/2016-02/23/c_1118133617.htm. Accessed on 29 August 2016

Xu G, Jiao L M, Zhao S L et al., 2016. Examining the impacts of land use on air quality from a spatio-temporal perspective in Wuhan, China. *Atmosphere*, 7(5): 62. doi: 10.3390/atmos7050062

Yan S M, Wu G, 2016. Network analysis of fine particulate Mmatter ($PM_{2.5}$) emissions in China. *Scientific Reports*, 6: 33227. doi: 10.1038/srep33227

Yang F M, Ye B M, He K B et al., 2005. Characterization of atmospheric mineral components of $PM_{2.5}$ in Beijing and Shanghai, China. *Science of the Total Environment,* 343(1): 221–230. doi: 10.1016/j.scitotenv.2004.10.017

Yin Qian, Wang Jingfeng, Hu Maogui et al., 2016. Estimation of daily $PM_{2.5}$ concentration and its relationship with meteorological conditions in Beijing. *Journal of Environmental Sciences,* 48: 161–168.doi: 10.1016/j.jes.2016.03.024

You W, Zang Z L, Zhang L F et al., 2016. National scale estimates of ground-level $PM_{2.5}$ concentration in China using geographically weighted regression based on 3 km resolution MODIS AOD. *Remote Sensing*, 8(3): 184. doi: 10.3390/rs8030184

Zhang Y L, Cao F, 2015. Fine particulate matter ($PM_{2.5}$) in China at a city level. *Scientific Reports*, 5: 14884. doi: 10.1038/srep14884